Received: 8 May 2023 | Revised: 3 August 2023 | Accepted: 31 October 2023

DOI: 10.1002/aic.18307

AIChE JOURNAL

RESEARCH ARTICLE

Soft Matter: Synthesis, Processing and Products

Nanoparticle transport in biomimetic polymer-linked emulsions

Daniel P. Keane | Colby J. Constantine | Matthew D. Mellor | Ryan Poling-Skutvik

Department of Chemical Engineering, University of Rhode Island, Kingstown, Rhode Island, USA

Correspondence
Ryan Poling-Skutvik, Department of Chemical Engineering, University of Rhode Island, Kingston, RI, USA.
Email: ryanps@uri.edu

Funding information
National Institute of General Medical Sciences, Grant/Award Number: P20GM103430

Abstract

The ability of nanoparticles to penetrate and transport through soft tissues is essential to delivering therapeutics to treat diseases or signaling agents for advanced imaging and sensing. Nanoparticle transport in biological systems, however, is challenging to predict and control due to the physicochemical complexity of tissues and biological fluids. Here, we demonstrate that nanoparticles suspended in a novel class of soft matter—polymer-linked emulsions (PLEs)—exhibit characteristics essential for mimicking transport in biological systems, including subdiffusive dynamics, non-Gaussian displacement distributions, and decoupling of dynamics from material viscoelasticity. Using multiple particle tracking, we identify the physical mechanisms underlying this behavior, which we attribute to a coupling of nanoparticle dynamics to fluctuations in the local network of polymer-linked droplets. Our findings demonstrate the potential of PLEs to serve as fully synthetic mimics of biological transport.

KEYWORDS
complex fluids, diffusion, microrheology, transport

1 | INTRODUCTION

The transport of chemical and biological species within the body controls the rate of biochemical reactions,[1-4] the efficacy and efficiency of delivering drugs to specific tissues or cancerous tumors,[5-8] and the propensity of pathogenic bacteria to penetrate mucosal layers.[9,10] Each transport process depends on a series of specific physicochemical interactions in combination with the local structure, dynamics, and viscoelasticity of the biological environment. Due to the inherent complexity of biological systems, however, it remains prohibitively challenging to predict how specific materials, chemicals, and biomacromolecules transport and accumulate within cells and tissues.

Nanoparticles serve as ideal probes with which to investigate biological transport because their small size mimics that of most biochemical species,[11,12] their geometry,[13-18] and their surface chemistry[19-21] can be easily modified, and they can be readily dyed or functionalized for facile detection.[22-24] In the absence of bulk flow, nanoparticle transport is driven by Brownian motion, in which thermal energy is balanced by viscous dissipation. In a homogeneous Newtonian fluid, Brownian motion is characterized by three properties: (1) a Gaussian distribution of particle displacements, (2) a mean-squared displacement that scales with time as $\langle \Delta \mathbf{r}^2 \rangle = 2dDt^{\beta}$, where d is the dimensionality of the system and $\beta = 1$ (i.e., Fickian), and (3) a diffusivity D that follows the Stokes–Einstein (SE) expression $D = k_B T/3\pi\eta d_H$, where η is the solution viscosity, d_H is the hydrodynamic diameter of the nanoparticle, and k_B is the Boltzmann constant.[25,26] Viscoelastic effects can be accounted for through the generalized Stokes-Einstein relationship (GSER), forming the foundation for microrheology[27-29] in which particle tracking experiments[30,31] identify local rheological properties. Biological systems, however, are often heterogeneous over the nanoparticle length scale and highly non-Newtonian. As a result, nanoparticle transport does not exhibit these three classical properties but is instead characterized by non-Gaussian distributions of particle displacements (DPDs), subdiffusive motion with $\beta < 1$, and faster-than-expected transport.[11,32-37] Although many theories have been proposed to explain such behavior, the underlying physical mechanisms remain poorly understood.

Acting as a boundary along free surfaces of the body, epithelial tissue plays a primary role in controlling the transport and penetration of nanoparticles into organs, such as the liver, kidneys, and spleen. Epithelial tissue is characterized by the tight packing of cells into single- or multilayer assemblies controlled by protein-mediated

intercellular adhesion.[38,39] Structurally, epithelial tissues contain cells on the order of 10 μm in diameter[40,41] and interstitial pores ranging from 1 to 100 nm in diameter.[34,42,43] The interstitial fluid contains a wide variety of glycosaminoglycans and proteoglycans[44] that aid cellular cohesion but also increase the viscosity of the interstitial fluid to slow nanoscale transport. The hierarchical structure of cells and interstitial voids leads to complex rheological properties. Previous work has characterized the viscoelastic moduli both *in vivo* and *ex vivo*, finding that epithelial and soft organ tissues have moduli ranging from 0.1 to 100 kPa.[45-48] While stiffer materials are expected to result in slower transport,[29] the heterogeneous structure of such tissues may allow particle transport to decouple from matrix viscoelasticity, resulting in transport occurring orders of magnitude more quickly than expected.[49,50] This interplay between viscoelasticity and structural heterogeneity makes it challenging to elucidate the specific physical mechanisms controlling nanoscale transport in these systems.

To address this challenge, researchers generate synthetic analogues of biological systems in which physicochemical interactions can be precisely controlled. Simple compartmentalization can be achieved with emulsion droplets in which surfactants stabilize a liquid-liquid interface.[51-53] Nanoparticle transport has been investigated in emulsions[54] and colloidal suspensions,[55,56] glassy systems,[57-60] and porous media,[61-63] broadly identifying a decrease in particle dynamics with increasing volume fraction ϕ of the dispersed phase, subdiffusivity at short length scales due to local caging, and deviations from the GSER when the nanoparticle diameter becomes smaller than the characteristic size of the dispersed phase. Additional complexity to synthetic systems can be introduced by modifying the liquid interface with polymers, lipids, and other functional groups[36,64-66] or through hierarchical compartmentalization.[67-69] Functionalized protocells can then be linked into a cohesive network by forming bilayers at the droplet-droplet interface[70-73] or through encapsulation within a hydrogel matrix.[74] Although these classes of synthetic soft materials capture the hierarchical arrangement and individual compartmentalization observed in cellularized tissues, they often fail to achieve the requisite mechanical elasticity. By contrast, polymeric systems lack compartmentalization but exhibit biomimetic mechanical properties arising from their underlying macromolecular structure. The transport of nanoparticles has been investigated in polymer solutions,[50,75-79] gels,[80-85] and melts.[49,86-88] Similar to dispersed systems, nanoparticle transport decreases with increasing polymer concentration and viscosity, becomes subdiffusive once the particles are localized within the polymer mesh, and begins to violate SE predictions when the nanoparticle size becomes smaller than the polymer radius of gyration R_g and correlation length ξ between chains. Gaining insight into biological transport, however, requires developing a synthetic biomimetic material that captures the viscoelastic network properties in combination with a distinct compartmentalized structure. By investigating nanoparticle transport in such a material, we can begin to understand the independent contributions from confinement in interstitial spaces and viscoelasticity.

Our previous work generated such a material by linking surfactant-stabilized emulsion droplets into a cohesive elastic network using high molecular weight telechelic triblock copolymers.[89,90] By changing the polymer molecular weight M_w and concentration, we create materials with elastic moduli ranging from 10 to 1000 Pa, comparable to that of soft tissues, and with interdroplet separations of approximately 30–40 nm[89] to mimic interstitial structures. In this article, we investigate nanoparticle transport in this novel biomimetic tissue analogue using optical microscopy and multiple particle tracking. Nanoparticle dynamics exhibit the essential properties observed for biological transport, including subdiffusion, decoupling of particle transport from local viscoelasticity, and non-Gaussian distributions of displacements. We characterize these properties using a combination of ensemble-averaged parameters and individual particle trajectories to demonstrate that nanoparticles transport by coupling to local fluctuations in cages of polymer-linked droplets. Our findings demonstrate the capability of PLEs to serve as effective biomimetic materials with which to investigate the mechanisms underlying transport within complex biological systems and soft tissues.

2 | MATERIALS AND METHODS

2.1 | Materials

Cyclohexane (≥ 99% purity), Tween 20, and Span 20 were purchased from Sigma Aldrich. Polystyrene-*b*-poly(ethylene oxide)-*b*-polystyrene (SEOS) of two different molecular weights were purchased from PolymerSource and were used without further modification. In this article, SEOS polymer nomenclature and polymer molecular weights are described according to SEOS-*X*/*Y*, where *X* and *Y* denote the number-average molecular weight M_n in kDa of the poly(ethylene oxide) (PEO) midblock and polystyrene (PS) endblocks, respectively. Fluorescent red and green poly(methyl methacrylate) (PMMA) nanoparticles ranging in diameter from 100 nm to 1 μm and stabilized with a carboxylate surface functionality were purchased from PolyAn and Lab261. Nominal sizes are provided by the suppliers, and measured sizes determined from particle tracking measurements in dilute (i.e., $\phi < 0.01$) emulsions are detailed in the Appendix S1.

2.2 | Emulsion preparation

Preparation of the polymer-linked nanoemulsions follows the procedure detailed in previous work.[89,90] Briefly, cyclohexane-in-water emulsions stabilized by a mixture of nonionic surfactants were prepared under sonication at a dispersed volume fraction of $\phi = 0.5$. The resulting emulsions contain a polydisperse distribution of cyclohexane droplets with an average hydrodynamic diameter of approximately 400 nm, as determined through dynamic light scattering. SEOS polymer was then added to the emulsions at a nominal concentration of 27 g/L (i.e., 3 wt%) and gently stirred at 50 °C until the polymer was fully dissolved. Nanoparticles were added to emulsions at volume fractions ranging from $\phi = 10^{-6}$ to 10^{-5} depending on size. The nanoparticles dispersed only in the continuous phase with no observable attachment to the droplet interface as confirmed by tracking measurements in the neat emulsion. For emulsions

containing SEOS, PMMA nanoparticles were added to the suspension either before (pre) or after (post) the polymer is dissolved. Emulsions remained stable for upwards of 2 weeks, and all emulsion characterization was conducted within a week of preparation.

2.3 | Rheology

Rheological characterizations of these emulsions were conducted on a TA Instruments HR-20 rheometer using either a 2° cone-and-plate geometry with a diameter of 20 mm or a concentric cylinder with a cup diameter of 30 mm and bob diameter of 28 mm. A solvent trap covered the sample for each geometry, and for the cone-and-plate geometry, the solvent trap was sealed with mineral oil and cyclohexane was added to the interior to minimize sample evaporation. The frequency range used to characterize the emulsions was chosen to ensure sufficient torque and to minimize inertial effects.

2.4 | Optical microscopy

Optical microscopy was conducted on a Leica DMi8 Inverted Microscope equipped with a Prime 95B Scientific CMOS (sCMOS) camera. Emulsions were imaged in sealed chambers prepared from glass slides and sealed with epoxy. Emulsions were imaged on a 40× air-immersion objective, which has a numerical aperture (NA) of 0.8, or on oil-immersion objectives of 63× (NA = 1.32) or 100× (NA = 1.4) using green and red filter cubes, depending on the color of the nanoparticle present. Videos were taken at frame rates ranging from 1 to 50 Hz, depending on particle dynamics. A minimum of five videos were taken of each sample at random positions to ensure appropriate statistics and sampling and to prevent photobleaching. A schematic of the emulsion structure containing fluorescent nanoparticles is shown in Figure 1. Note that this schematic shows a simplified system, only depicting the chains in bridging conformations and omitting those in looping conformations.

2.5 | Particle tracking

Microscope videos were processed using an in-house MATLAB code that implements a centroid-based tracking algorithm[30] to generate particle trajectories. From these trajectories, we calculate the one-dimensional, ensemble-averaged mean-squared displacement (MSD)

$$\langle \Delta x^2(\Delta t)\rangle = \sum_i^N (x_i(t+\Delta t)-x_i(t))^2 - \left(\sum_i^N x_i(t+\Delta t)-x_i(t)\right)^2, \quad (1)$$

where the second sum corrects for bulk flow. One-dimensional MSDs are used in place of two-dimensional calculations for simplicity, and we verify that the dynamics are equal in the x and y directions (Appendix S1). MSDs are computed by combining the trajectories from each video, and the error is estimated by taking the standard deviations (SDs) of MSDs calculated for individual videos. By identifying the particle centroids, the tracking algorithm achieves sub-pixel resolution of approximately $\varepsilon \approx 50$ nm with a 100× objective, $\varepsilon \approx 80$ nm with a 63× objective, and $\varepsilon \approx 125$ nm with a 40× objective. The calculated MSD is then fit to a power-law

$$\langle \Delta x^2(\Delta t)\rangle = 2D\Delta t^{\beta}, \quad (2)$$

where β characterizes the nature of nanoparticle transport with $\beta = 1$ corresponding to Fickian diffusion with a diffusivity D and $\beta < 1$ signifying subdiffusion. In addition to MSDs, we calculate DPDs through a one-dimensional self van Hove distribution[91]

$$G_s(\Delta x, \Delta t) = N^{-1}\left\langle \sum_i^N \delta(x_i(t)-x_i(t+\Delta t)-\Delta x)\right\rangle, \quad (3)$$

where δ is the Dirac delta and N is the total number of particles. For diffusive particles undergoing Gaussian displacements,

$$G_s(\Delta x, \Delta t) = \frac{1}{\sqrt{2\pi\langle \Delta x^2(\Delta t)\rangle}} \exp\left(-\frac{\Delta x^2}{2\langle \Delta x^2(\Delta t)\rangle^2}\right). \quad (4)$$

For non-Gaussian processes, the DPD is characterized by a non-Gaussian parameter

$$\alpha = \frac{\langle \Delta x^4(\Delta t)\rangle}{3\langle \Delta x^2(\Delta t)\rangle^2} - 1, \quad (5)$$

which quantifies the deviation of the DPD from a Gaussian distribution. For non-directed Brownian motion in a Newtonian fluid, α should

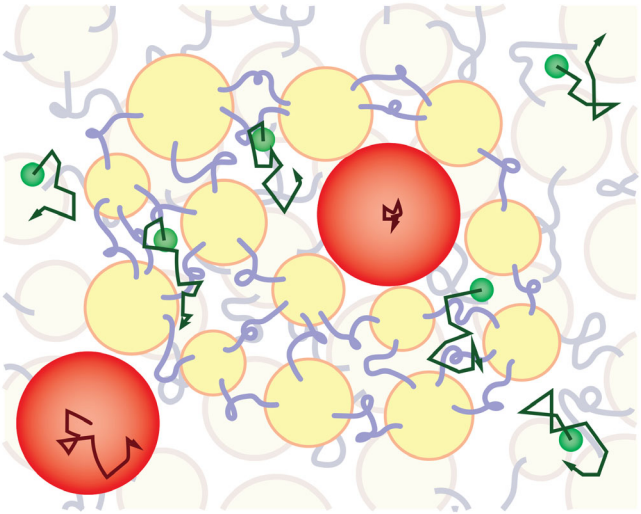

FIGURE 1 Schematic illustrating the structure of the polymer-linked emulsions, with emulsion droplets in yellow and bridging triblock copolymers in blue. Identified particle trajectories show large particles (red) exhibiting confined behavior and small particles (green) transporting through the interstitial spaces. Not drawn to scale.

be 0, indicating a normal distribution of particle displacements. Higher values of α (i.e., $\alpha > 0$) indicate deviations from Gaussian behavior.

3 | RESULTS AND DISCUSSION

3.1 | Emulsion characterization

The structure and rheological properties of polymer-linked emulsions (PLEs) are governed by the concentration and M_w of the telechelic triblock copolymers.[89,90] Here, we use two different polymers—SEOS-180/32, which has high-M_w mid- and endblocks, and SEOS-27/11.5, which has low-M_w blocks—to generate emulsions with comparable rheology but different structures. The rheological properties of these PLEs and a neat emulsion are shown in Figure 2. The neat emulsion at $\phi = 0.5$ exhibits the expected properties for a viscoelastic fluid in which the viscous modulus G" increases with frequency ω and is larger than the elastic modulus G'. By contrast, both PLEs exhibit significantly enhanced elasticity relative to the neat emulsion with G' > G" and a weaker dependence on ω. This elasticity originates from the network of droplets linked by bridging polymers. Because the high-M_w midblocks experience less of an entropic penalty when forming a bridge,[92] the SEOS-180/32 sample contains a significantly higher fraction of total polymer chains in the bridging state. By contrast, the low-M_w SEOS-27/11.5 polymer has fewer relative bridges but many more total chains in the material due to the lower M_w. The decreased bridging fraction is offset by the increased number of total chains, resulting in a cohesive network with comparable viscoelastic moduli and relaxation spectra. Despite this rheological similarity, confocal microscopy demonstrates that the PLEs possess different structures when prepared using the different polymeric linkers.[90] SEOS-180/32 creates a percolated network with homogeneous bridging density, whereas the SEOS-27/11.5 sample possesses a heterogeneous network in which bridges are concentrated within clusters of droplets, and the clusters are weakly bound together by a small number of bridges. Thus, these emulsions provide a controlled system in which we can evaluate changes to nanoparticle transport arising from emulsion structure and viscoelasticity separately.

3.2 | Nanoparticle transport

We begin by evaluating nanoparticle transport in neat emulsions with $\phi = 0.5$ for nanoparticles with varying hydrodynamic diameters (Figure 3). In the absence of polymers, the emulsion behaves like a viscoelastic shear-thinning fluid. As a result, the nanoparticles exhibit diffusive transport in which their MSD increases linearly with time. We fit the MSDs to Equation (2) with $\beta = 1$ to extract D as a function of particle size (inset to Figure 3). We observe that $D \sim d_H^{-1}$, in good agreement with the predicted SE behavior. The DPDs are Gaussian for all particle sizes, confirming Fickian diffusion (Appendix S1). Based on these results, we find that nanoparticles transport through the neat emulsion as expected with a diffusivity that is coupled to the emulsion viscosity.

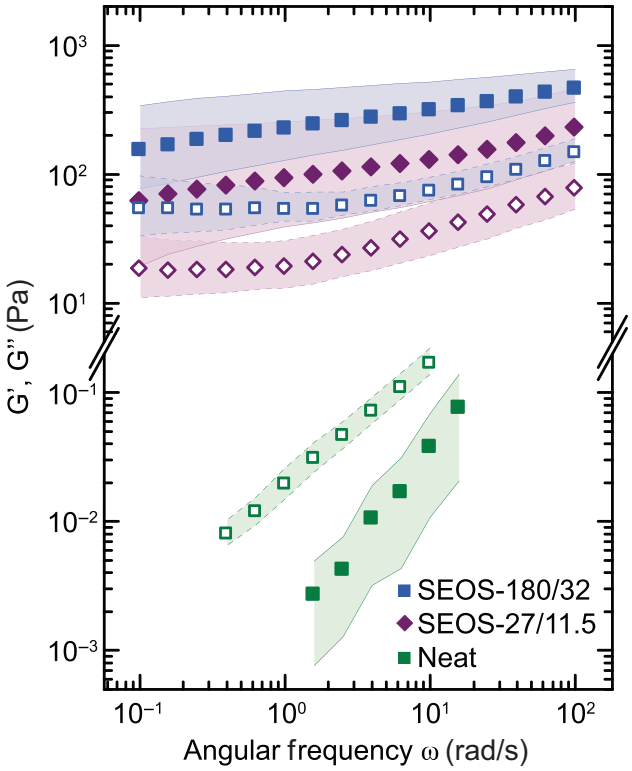

FIGURE 2 Storage modulus G' (closed) and loss modulus G" (open) as a function of oscillation frequency ω for a neat emulsion and for emulsions containing 27 g/L of SEOS-180/32 or SEOS-27/11.5. Shaded regions represent the standard deviation measured across samples.

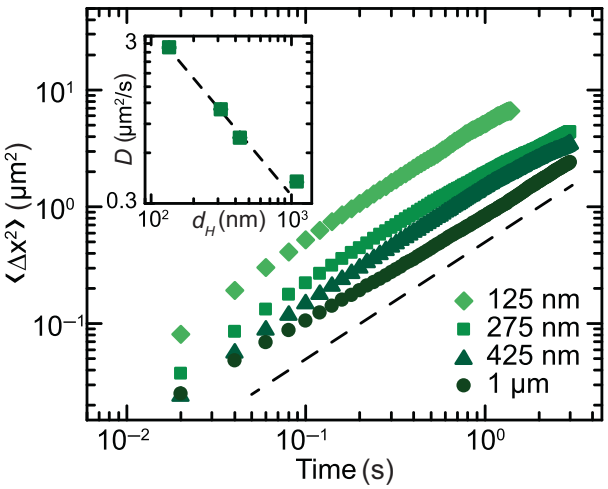

FIGURE 3 Mean-squared displacement $\langle \Delta x^2 \rangle$ in a neat emulsion at $\phi = 0.5$ as a function of time Δt for nanoparticles of varying size. Dashed line represents $\langle \Delta x^2 \rangle \sim \Delta t^1$ scaling. *Inset*: Diffusivity D as a function of particle size. Dashed line represents $D \sim d_H^{-1}$ scaling.

In the PLEs, however, nanoparticle transport becomes significantly more complex (Figure 4). Whereas nanoparticles moved diffusively in the neat emulsion, they move subdiffusively in PLEs on short time scales with $\beta < 1$ for all particle diameters and polymer molecular

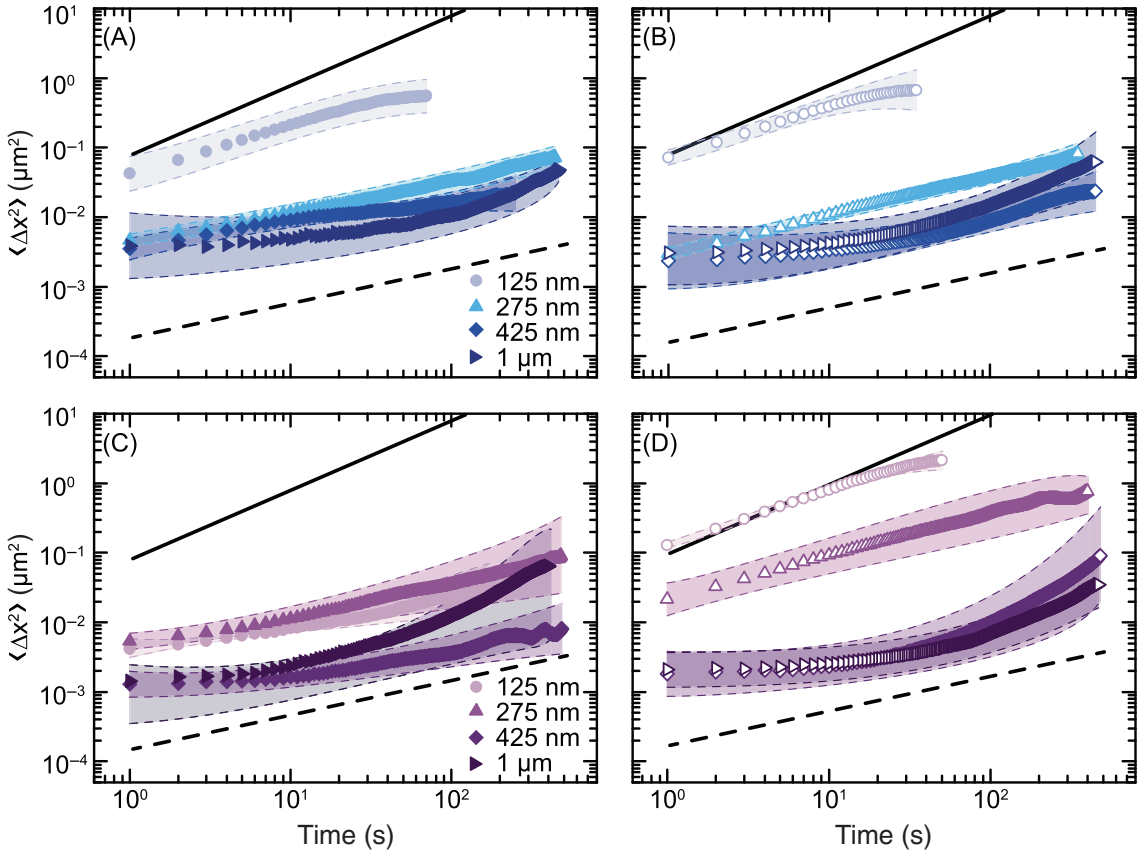

FIGURE 4 Mean-squared displacement $\langle \Delta x^2 \rangle$ as a function of time Δt for nanoparticles of varying sizes suspended in polymer-linked emulsions containing (A, B) SEOS-180/32 and (C, D) SEOS-27/11.5. Nanoparticles are added (A, C) prior to or (B, D) after polymer. Solid and dashed lines show scaling for $\beta = 1$ and 0.5, respectively. Error bands indicate one SD between videos for a given sample. (A) SEOS-180/32 Pre; (B) SEOS-180/32 Post; (C) SEOS-27/11.5 Pre; (D) SEOS-27/11.5 Post.

weights. Additionally, we observe multiple broad trends in the ensemble-averaged MSDs. First, smaller nanoparticles tend to be more dynamic than larger nanoparticles, although experimental variability leads to some deviations between samples. For example, in the SEOS-180/32 samples, the 125 nm particles transport over an order of magnitude faster than the 1 μm particles. This enhanced transport of small nanoparticles can be partly explained through the explicit size dependence of the SE expression but may also reflect additional contributions from the coupling of nanoparticle dynamics to local fluctuations of either the polymer[50,77,79] or the emulsion.[57,60] Second, particle dynamics can depend on whether the particles are added before or after the polymer. For the high-M_w SEOS-180/32 emulsions, there is no statistically significant difference between the dynamics of pre- or post-addition particles. In emulsions containing the low-M_w SEOS-27/11.5, however, small nanoparticles transport orders of magnitude faster when added after the polymer while the dynamics of larger particles remain largely unchanged. Because the moduli of these emulsions are comparable, this difference in nanoparticle transport must originate from the structural or mechanical heterogeneities of the polymer-mediated droplet network. We hypothesize that when small nanoparticles are added prior to the polymer, they are uniformly distributed throughout the material and subsequently trapped as the polymer forms bridges between droplets to form a local cage. When added after the polymer, however, the nanoparticles preferentially penetrate and localize within regions of reduced polymer concentration, resulting in more rapid transport. Large particles are less sensitive to this structural heterogeneity because the emulsion structure averages over the nanoparticle surface. Because the SEOS-27/11.5 polymer generates tightly bound clusters of droplets, there is a larger difference between the dynamics of particles added before and after the polymer than in the SEOS-180/32 samples, which possess a more homogeneous network structure.

To discuss these trends more quantitatively, we compare the magnitudes of particle MSDs at $\Delta t = 10$ s (Figure 5). We choose this metric as a proxy for the rate of nanoparticle transport for two reasons. First, the MSDs are subdiffusive, meaning that the diffusivity D is poorly defined. Second, this timescale is sufficiently long to resolve particle motion above the resolution of the tracking algorithm while simultaneously retaining sufficient statistics. In general, the MSD values decrease with increasing particle size, but the scaling of this change disagrees with predictions from GSER. The GSER predicts that particles moving in a viscoelastic medium should exhibit a d_H^{-1} scaling.[29] We observe a more rapid decrease in transport with increasing particle size, instead approaching a power-law scaling of -2. This discrepancy between predicted and observed behavior indicates that

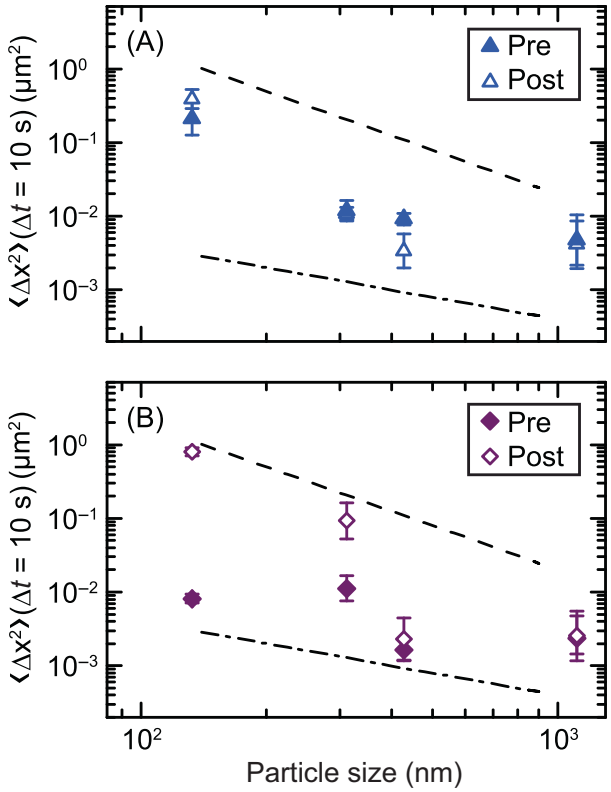

FIGURE 5 Mean-squared displacement (MSD) of nanoparticles at $\Delta t = 10$ s as a function of nanoparticle size in polymer-linked emulsions (PLEs) containing (A) SEOS-180/32 and (B) SEOS-27/11.5 and for particles added pre- (closed) and post-polymer addition (open). Dashed lines correspond to a d_H^{-2} scaling, and dash-dot lines correspond to d_H^{-1} scaling. Error bars indicate one SD between videos.

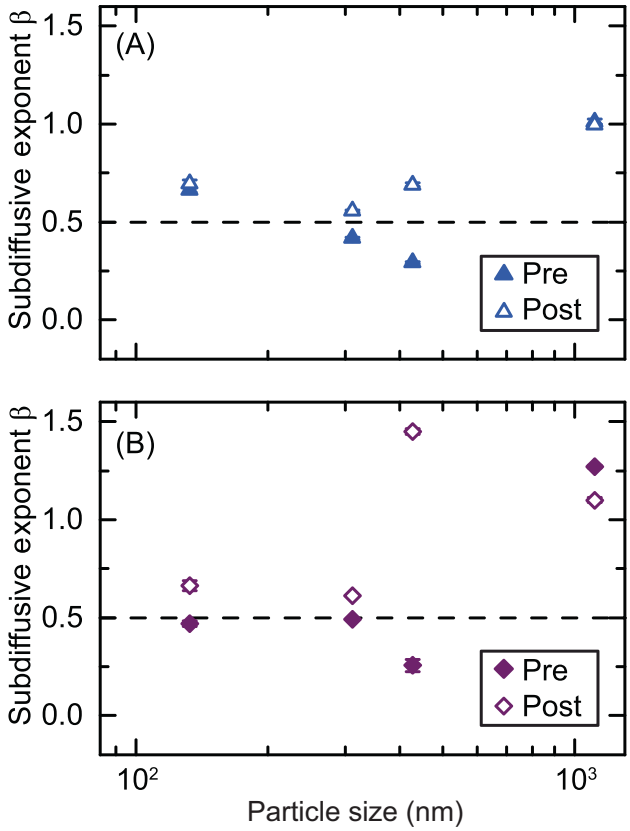

FIGURE 6 Subdiffusive exponent β as a function of nanoparticle size in polymer-linked emulsions (PLEs) containing (A) SEOS-180/32 and (B) SEOS-27/11.5 for particles added pre- (closed) and post-polymer addition (open). Dashed lines indicate the predicted $\beta = 0.5$ for particles fully coupled to the Rouse relaxations of polymers. Error bars indicate 95% confidence intervals on the fitting parameters.

small nanoparticles transport more rapidly through PLEs than expected based on local viscoelasticity, in agreement with earlier studies on nanoparticles in heterogeneous soft materials[57,77] and biological materials.[34] Additionally, within experimental error, there is no significant difference between the MSD values for nanoparticles added prior to or after the addition of SEOS-180/32, suggesting that nanoparticles are able to fully sample and penetrate the SEOS-180/32 PLE network. By contrast, the dynamics of particles suspended in the SEOS-27/11.5 PLE depend strongly on whether the nanoparticles are added before or after the polymer. The nanoparticles added prior to SEOS-27/11.5 all show $\langle \Delta x^2(\Delta t = 10\,s) \rangle \approx 0.002 - 0.02\ \mu m^2$ with a weak size dependence. These MSD values are comparable to the resolution $\varepsilon^2 \approx 0.0025\ \mu m^2$ of our tracking algorithm, suggesting that particles in this system are irreversibly trapped within the dense clusters of droplets. When added after the SEOS-27/11.5 polymer, smaller particles transport more rapidly than larger particles, consistent with the dynamics in the SEOS-180/32 PLEs, and with a stronger size-dependence than the SE prediction. Overall, these ensemble-averaged MSDs demonstrate that nanoparticle transport decouples from bulk rheology in PLEs, violating the GSER, and instead depends on the specific structure and properties of the emulsion.

3.3 | Transport mechanisms

Although these ensemble-averaged MSDs provide insight into the complexity of nanoparticle transport in PLEs, they do not identify the underlying physical mechanisms controlling this behavior. To begin to understand these mechanisms, we investigate the degree of subdiffusion by fitting the MSD to Equation (2) (Figure 6). We fit over regions exhibiting prolonged power-law behaviors, corresponding to shorter timescales for small, mobile particles (i.e., timescales ranging from ~1 to 30 s) but longer timescales for larger, slower particles (i.e., timescales ranging from ~50 to 300 s). We observe surprising trends of the subdiffusive exponent β with particle size in both the high-M_w and low-M_w emulsions and as a function of pre- or postaddition. For both polymers, β values are low, ranging from $\beta \approx$ 0.5–0.7 when the nanoparticles are smaller than the emulsion droplets (i.e., <400 nm). These β values are consistent with earlier studies on nanoparticles suspended in unentangled polymer solutions[77] or chemically bound to polymer networks[93] in which the nanoparticles couple to the Rouse relaxations of the surrounding polymers.[94] In these PLE systems, we expect that this coupling mode arises as particles are locally caged within polymer-linked clusters. This idea is further supported by the

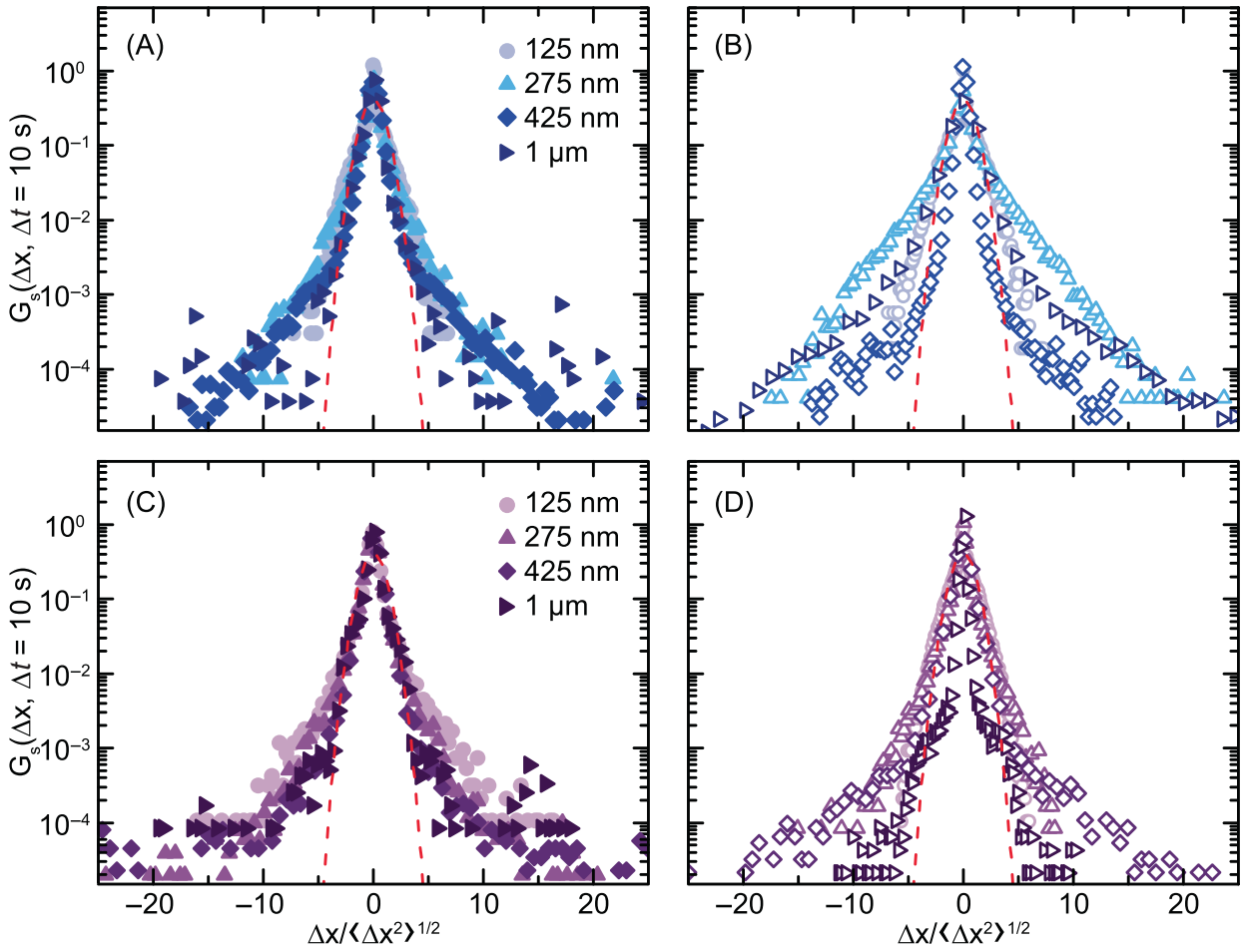

FIGURE 7 Distributions of particle displacements (DPDs) as a function of normalized distance $\Delta x/\left(\langle \Delta x^2 \rangle\right)^{1/2}$ at $\Delta t = 10$ s for nanoparticles of varying sizes suspended in polymer-linked emulsions (PLEs) containing (A, B) SEOS-180/32 and (C, D) SEOS-27/11.5. Nanoparticles are added (A, C) prior to or (B,D) after polymer. The dashed red curves represent Gaussian predictions. (A) SEOS-180/32 Pre; (B) SEOS-180/32 Post; (C) SEOS-27/11.5 Pre; (D) SEOS-27/11.5 Post.

smaller β values observed for preaddition nanoparticles than for post-addition particles. In the preaddition samples, nanoparticles are more equally distributed throughout the sample and are thereby more likely to reside within these polymer-linked clusters than those added after the polymer.

For particles larger than the emulsion droplets, however, we observe deviations from the $\beta \approx 0.5$ condition. For the 425 nm particles, we observe $\beta < 0.5$ when the particles are added prior to the polymer, indicating stronger confinement of the particles, but $\beta > 0.5$ when added after the polymer, suggesting that the particles are able to transport more diffusively. For the largest 1 μm particles, we observe $\beta \geq 1$ that correspond to diffusive transport. Combined with the long timescales over which these β values are extracted, we attribute the higher β values to particles coupling to droplet relaxations rather than polymer fluctuations. These diffusive escapes from local cages is strongly reminiscent of the dynamics observed in glassy colloidal liquids in which particles are locally caged by their nearest neighbors but become diffusive on long timescales as these structural cages relax.[95,96] Overall, these β values suggest that there are competing mechanisms governing how nanoparticles transport in PLEs. Small nanoparticles are sensitive to the fluctuations of their local cage and couple to the segmental relaxations of the bridging polymer. Large nanoparticles, however, remain caged on short timescales and eventually transport by coupling to the glassy relaxations of the droplets.

As further evidence that particle transport is coupled to relaxations in the surrounding PLE, the DPDs exhibit non-Gaussian signatures with narrow peaks at $\Delta x = 0$ and extended tails at large absolute values of Δx (Figure 7). We normalize the displacement Δx by the square-root of the MSD to compare the dynamics of particles of different sizes and in different samples. For a Gaussian process, this normalization would collapse the data onto a single curve, as observed in neat emulsions (Appendix S1). By contrast, we observe significant differences in the shapes of the distributions as a function of particle size and sample. The sharp peaks at $\Delta x = 0$ observed for some samples likely reflect the resolution of our tracking algorithm, which acts as a lower bound on the magnitude of particle motion we can detect above experimental noise.[31] Even for these samples, however, we

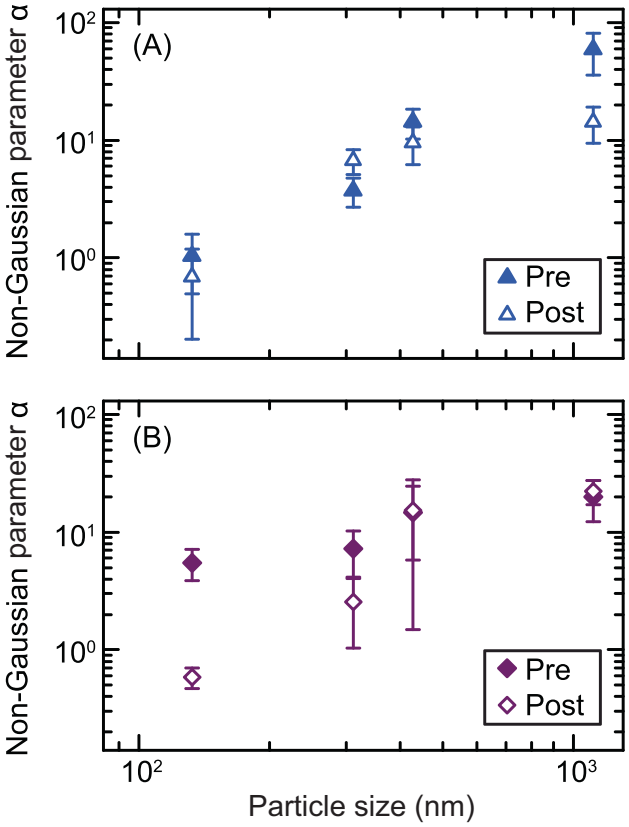

FIGURE 8 Non-Gaussian parameter α calculated at $\Delta t = 10$ s as a function of nanoparticle size in polymer-linked emulsions (PLEs) containing (A) SEOS-180/32 and (B) SEOS-27/11.5 and for particles added pre- (closed) and post-polymer addition (open). Error bars indicate one SD between videos.

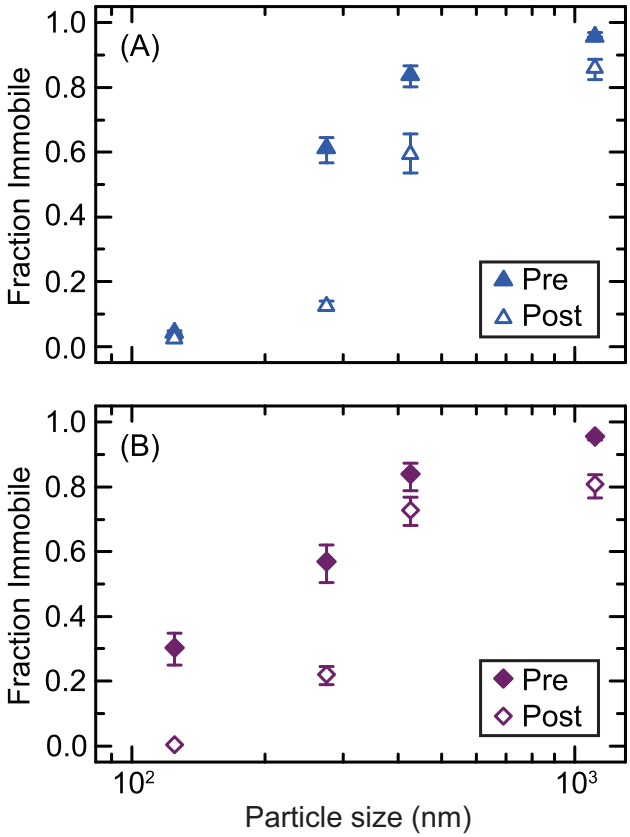

FIGURE 9 Fraction of particles that are immobile as a function of nanoparticle size in polymer-linked emulsions (PLEs) containing (A) SEOS-180/32 and (B) SEOS-27/11.5 and for particles added pre- (closed) and post-polymer addition (open). Error bars indicate the range of immobile fractions calculated across one SD in the resolution cutoff.

observe a significant population of displacements occurring on larger distances commensurate with nanoparticle motion beyond the resolution limit.

We quantify changes in the shape of these DPDs through the non-Gaussian parameter α (Figure 8). For the neat emulsions, $\alpha \approx 0$ for all particle sizes, indicating a normal distribution of particle displacements (Appendix S1). In PLEs, however, we observe $\alpha > 0$, confirming that nanoparticle transport occurs through non-Gaussian processes. Non-Gaussian dynamics are widely observed in complex materials[55,97-99] and are commonly associated with a distribution of diffusivities[55,100,101] arising from a variety of physical mechanisms including structural heterogeneities, spatiotemporal variations in hydrodynamic interactions, or the formation and breaking of transient cages. For PLEs, we expect that the distribution of diffusivities is largely controlled by the structural heterogeneities introduced by differences in bridging distributions and local cages being formed by the linked droplets. Thus, we attribute the nonzero α-values to particles experiencing heterogeneities and transient caging. Generally, α increases with particle size as particles become less mobile and more localized within polymer-linked cages. We do note that for the largest 1 μm particles, α captures contributions from the tracking algorithm peak at $\Delta x = 0$ and that the true value of α may be lower. For the high-M_w SEOS-180/32 samples, there is no difference in α for particles added before or after the polymer, consistent with the behavior of the MSDs. By contrast, the pre-polymer particles in the low-M_w SEOS-27/11.5 samples exhibit larger α for small particle sizes than in the post-polymer systems but comparable values at larger particle sizes. This behavior again qualitatively agrees with the observed trends in particle MSDs and confirms that the dynamics of small particles are sensitive to the structural heterogeneities present in the SEOS-27/11.5 samples.

The non-Gaussian DPDs and small values of MSDs in these PLEs suggest that a significant population of nanoparticles are caged within the network of polymer-linked droplets. We quantify this population of immobile particles by identifying particles in which the individual mean-squared displacement $\langle \Delta x^2(\Delta t = 10\,\text{s}) \rangle < \varepsilon^2$, where ε is the resolution of our tracking algorithm. This definition effectively separates mobile and immobile populations (see Appendix S1) and is comparable to the definition used for quantum dots transporting through a polymeric hydrogel.[84] Using this definition, we find that small nanoparticles are mostly mobile while the majority of large particles are immobile in all PLE materials (Figure 9). The fraction of immobile particles increases with particle size with a dramatic increase once the

particles become comparable in size to the surrounding droplets. Additionally, we observe that there is a significant immobile fraction for even the smallest 125 nm particles in SEOS-27/11.5 PLEs when added prior to the polymer. This large immobile fraction of small nanoparticles is consistent with the suppressed MSDs and larger values of α observed in this system and further reinforces our understanding that this low-M_w polymer generates dense clusters of polymer-linked droplets. When particles are added after the SEOS-27/11.5 polymer, however, the majority of 125 nm particles are mobile, indicating that the nanoparticles remain in regions with reduced polymer concentration and do not penetrate the dense clusters. Surprisingly, we observe a similar trend for the emulsions containing SEOS-180/32. While the MSDs and α values are indistinguishable for particles added before or after the SEOS-180/32 polymer, we observe consistently higher fractions of immobile particles for the pre-addition system. This larger immobile fraction suggests that nanoparticles are experiencing structural heterogeneities but less frequently than in the SEOS-27/11.5 sample. Furthermore, these heterogeneities are not detectable through ensemble-averaged parameters—$\langle \Delta x^2 \rangle$, β, and α—but only appear when looking at individual particle trajectories. This sensitivity suggests that the immobile fraction and analysis of individual MSDs may be more sensitive to characterizing the structural heterogeneities present in complex fluids and biomimetic materials.

4 | CONCLUSION

We use optical microscopy and particle tracking to investigate the transport of nanoparticles in a novel biomimetic system comprised of PLE droplets. By varying the polymer M_w, we produce systems with comparable viscoelastic moduli but different microscale morphologies that effectively control nanoparticle transport to replicate the complexity observed in many biological systems. Specifically, we observe subdiffusive transport, MSDs that decrease more rapidly with nanoparticle size than predicted by the Stokes–Einstein expression, and non-Gaussian displacement distributions. These metrics demonstrate that nanoparticle transport in PLEs is largely controlled by the coupling of nanoparticle dynamics to fluctuations of structural heterogeneities within the local environment; particles smaller than the droplet diameter couple to fluctuations of the polymer chains whereas larger particles couple to droplet relaxations. We expect that these structural heterogeneities arise from differences in the spatial distributions of polymer bridges and transient caging induced by the polymer-linked droplets. Indeed, the fraction of immobile particles increases with increasing particle size as they become more strongly caged within the network structure. Our findings demonstrate that these PLE materials not only mimic the rheological properties of soft tissues but also generate biologically relevant transport. As such, we expect that PLEs can be used as *in vitro* models of biological tissues to identify physical mechanisms underlying the performance of targeted drug delivery vectors[7,8,102] and nanotherapeutics.[103-105] Specifically, PLE materials can provide a well-controlled synthetic environment in which we can assess the role of interparticle interactions, transient binding, particle shape, and composition of interstitial fluid on the ability of nanoparticles, liposomes, and other species to penetrate and accumulate within soft tissues. Future work will seek to mimic the deformability and unique surface chemistries of nanotherapeutics by using compressible liposomes and functionalized tracers. Additionally, we aim to extend our investigation to even smaller particle sizes to better access the relevant length scales for targeted drug delivery techniques.

AUTHOR CONTRIBUTIONS

Daniel P. Keane: conceptualization (supporting); formal analysis (lead); investigation (lead); methodology (supporting); resources (lead); software (lead); visualization (lead); writing – original draft (supporting); writing – review and editing (equal). **Colby J. Constantine:** formal analysis (supporting); investigation (supporting); visualization (supporting); writing – review and editing (supporting). **Matthew D. Mellor:** formal analysis (supporting); investigation (supporting); visualization (supporting); writing – review and editing (supporting). **Ryan Poling-Skutvik:** conceptualization (lead); formal analysis (supporting); funding acquisition (lead); methodology (lead); project administration (lead); supervision (lead); writing – original draft (lead); writing – review and editing (equal).

ACKNOWLEDGMENTS

This work was fully supported by the Rhode Island Institutional Development Award (IDeA) Network of Biomedical Research Excellence from the National Institute of General Medical Sciences of the National Institutes of Health under grant number P20GM103430.

DATA AVAILABILITY STATEMENT

The data that support the findings of this study are available from the corresponding author upon reasonable request.

ORCID

Ryan Poling-Skutvik https://orcid.org/0000-0002-1614-1647

REFERENCES

1. Stiehl O, Weidner-Hertrampf K, Weiss M. Macromolecular crowding impacts on the diffusion and conformation of DNA hairpins. *Phys Rev E*. 2015;91(1):012703. doi:10.1103/PhysRevE.91.012703
2. Minton AP. The influence of macromolecular crowding and macromolecular confinement on biochemical reactions in physiological media. *J Biol Chem*. 2001;276(14):10577-10580. doi:10.1074/jbc.R100005200
3. Jun SK, Yethiraj A. Effect of macromolecular crowding on reaction rates: a computational and theoretical study. *Biophys J*. 2009;96(4):1333-1340. doi:10.1016/j.bpj.2008.11.030
4. Miermont A, Waharte F, Hu S, et al. Severe osmotic compression triggers a slowdown of intracellular signaling, which can be explained by molecular crowding. *Proc Natl Acad Sci U S A*. 2013;110(14):5725-5730. doi:10.1073/pnas.1215367110
5. Singh R, Lillard JW. Nanoparticle-based targeted drug delivery. *Exp Mol Pathol*. 2009;86(3):215-223. doi:10.1016/j.yexmp.2008.12.004
6. Bae YH, Park K. Targeted drug delivery to tumors: myths, reality and possibility. *J Control Release*. 2011;153(3):198-205. doi:10.1016/j.jconrel.2011.06.001

7. Tang L, Yang X, Yin Q, et al. Investigating the optimal size of anticancer nanomedicine. *Proc Natl Acad Sci*. 2014;111(43):15344-15349. doi:10.1073/pnas.1411499111
8. Liu Y, Castro Bravo KM, Liu J. Targeted liposomal drug delivery: a nanoscience and biophysical perspective. *Nanoscale Horiz*. 2021;6(2):78-94. doi:10.1039/D0NH00605J
9. Celli JP, Turner BS, Afdhal NH, et al. *Helicobacter pylori* moves through mucus by reducing mucin viscoelasticity. *Proc Natl Acad Sci U S A*. 2009;106(34):14321-14326. doi:10.1073/pnas.0903438106
10. Hansson GC. Role of mucus layers in gut infection and inflammation. *Curr Opin Microbiol*. 2012;15(1):57-62. doi:10.1016/j.mib.2011.11.002
11. Kalwarczyk T, Tabaka M, Holyst R. Biologistics–diffusion coefficients for complete proteome of Escherichia Coli. *Bioinformatics*. 2012;28(22):2971-2978. doi:10.1093/bioinformatics/bts537
12. Mosquera J, Garcia I, Liz-Marzán LM. Cellular uptake of nanoparticles versus small molecules: a matter of size. *Acc Chem Res*. 2018;51(9):2305-2313. doi:10.1021/acs.accounts.8b00292
13. Li Y, Wu Y, Ong BS. Facile synthesis of silver nanoparticles useful for fabrication of high-conductivity elements for printed electronics. *J Am Chem Soc*. 2005;127(10):3266-3267. doi:10.1021/ja043425k
14. McGilvray KL, Decan MR, Wang D, Scaiano JC. Facile photochemical synthesis of unprotected aqueous gold nanoparticles. *J Am Chem Soc*. 2006;128(50):15980-15981. doi:10.1021/ja066522h
15. Hartlen KD, Athanasopoulos PT, Kitaev V. Facile preparation of highly monodisperse small silica spheres (15 to >200 nm) suitable for colloidal templating and formation of ordered arrays. *Langmuir*. 2008;24(16):1714-1720. doi:10.1021/la7025285
16. Ye X, Jin L, Caglayan H, et al. Improved size-tunable synthesis of monodisperse gold Nanorods through the use of aromatic additives. *ACS Nano*. 2012;6(3):2804-2817. doi:10.1021/nn300315j
17. Ye X, Zheng C, Chen J, Gao Y, Murray CB. Using binary surfactant mixtures to simultaneously improve the dimensional tunability and monodispersity in the seeded growth of gold nanorods. *Nano Lett*. 2013;13(2):765-771. doi:10.1021/nl304478h
18. Kuttner C, Mayer M, Dulle M, et al. Seeded growth synthesis of gold nanotriangles: size control, SAXS analysis, and SERS performance. *ACS Appl Mater Interfaces*. 2018;10(13):11152-11163. doi:10.1021/acsami.7b19081
19. Howes PD, Chandrawati R, Stevens MM. Colloidal nanoparticles as advanced biological sensors. *Science*. 2014;346(6205):1247390. doi:10.1126/science.1247390
20. Poling-Skutvik R, Slim AH, Narayanan S, Conrad JC, Krishnamoorti R. Soft interactions modify the diffusive dynamics of polymer-grafted nanoparticles in solutions of free polymer. *ACS Macro Lett*. 2019;8(8):917-922. doi:10.1021/acsmacrolett.9b00294
21. Hore MJA. Polymers on nanoparticles: structure & dynamics. *Soft Matter*. 2019;15(6):1120-1134. doi:10.1039/C8SM02110D
22. Burns A, Ow H, Wiesner U. Fluorescent core-shell silica nanoparticles: towards "lab on a particle" architectures for nanobiotechnology. *Chem Soc Rev*. 2006;35:1028-1042. doi:10.1039/b600562b
23. Chauhan VP, Popović Z, Chen O, et al. Fluorescent nanorods and nanospheres for real-time in vivo probing of nanoparticle shape-dependent tumor penetration. *Angew Chem*. 2011;123(48):11619-11622. doi:10.1002/ange.201104449
24. Cong L, Takeda M, Hamanaka Y, et al. Uniform silica coated fluorescent nanoparticles: synthetic method, improved light stability and application to visualize lymph network tracer. *PloS One*. 2010;5(10):e13167. doi:10.1371/journal.pone.0013167
25. Einstein A. Über die von der molekularkinetischen theorie der wärme geforderte bewegung von in ruhenden flüssigkeiten suspendierten teilchen. *Ann Phys*. 1905;322(8):549-560. doi:10.1002/andp.19053220806
26. von Smoluchowski M. Zur kinetischen theorie der brownschen molekularbewegung und der suspensionen. *Ann Phys*. 1906;326(14):756-780. doi:10.1002/andp.19063261405
27. Mason TG, Weitz DA. Optical measurements of frequency-dependent linear viscoelastic moduli of complex fluids. *Phys Rev Lett*. 1995;74(7):1250-1253. doi:10.1103/PhysRevLett.74.1250
28. Crocker JC, Valentine MT, Weeks ER, et al. Two-point microrheology of inhomogeneous soft materials. *Phys Rev Lett*. 2000;85(4):888-891. doi:10.1103/PhysRevLett.85.888
29. Squires TM, Mason TG. Fluid mechanics of microrheology. *Annu Rev Fluid Mech*. 2010;42(1):413-438. doi:10.1146/annurev-fluid-121108-145608
30. Crocker JC, Grier DG. Methods of digital video microscopy for colloidal studies. *J Colloid Interface Sci*. 1996;179(1):298-310. doi:10.1006/jcis.1996.0217
31. Rose KA, Molaei M, Boyle MJ, Lee D, Crocker JC, Composto RJ. Particle tracking of nanoparticles in soft matter. *J Appl Phys*. 2020;127(19):191101. doi:10.1063/5.0003322
32. Lai SK, O'Hanlon DE, Harrold S, et al. Rapid transport of large polymeric nanoparticles in fresh undiluted human mucus. *Proc Natl Acad Sci U S A*. 2007;104(5):1482-1487. doi:10.1073/pnas.0608611104
33. Mansfield ED, Sillence K, Hole P, Williams AC, Khutoryanskiy VV. POZylation: a new approach to enhance nanoparticle diffusion through mucosal barriers. *Nanoscale*. 2015;7(32):13671-13679. doi:10.1039/C5NR03178H
34. Nance EA, Woodworth GF, Sailor KA, et al. A dense poly(ethylene glycol) coating improves penetration of large polymeric nanoparticles within brain tissue. *Sci Transl Med*. 2012;4(149):149ra119. doi:10.1126/scitranslmed.3003594
35. Höfling F, Franosch T. Anomalous transport in the crowded world of biological cells. *Rep Prog Phys*. 2013;76(4):046602. doi:10.1088/0034-4885/76/4/046602
36. Weiss M, Frohnmayer JP, Benk LT, et al. Sequential bottom-up assembly of mechanically stabilized synthetic cells by microfluidics. *Nat Mater*. 2018;17(1):89-95. doi:10.1038/NMAT5005
37. Cherstvy AG, Thapa S, Wagner CE, Metzler R. Non-Gaussian, non-ergodic, and non-Fickian diffusion of tracers in mucin hydrogels. *Soft Matter*. 2019;15(12):2526-2551. doi:10.1039/c8sm02096e
38. Farhadifar R, Röper JC, Aigouy B, Eaton S, Jülicher F. The influence of cell mechanics, cell-cell interactions, and proliferation on epithelial packing. *Curr Biol*. 2007;17(24):2095-2104. doi:10.1016/j.cub.2007.11.049
39. Cohen DJ, Gloerich M, Nelson WJ. Epithelial self-healing is recapitulated by a 3D biomimetic E-cadherin junction. *Proc Natl Acad Sci U S A*. 2016;113(51):14698-14703. doi:10.1073/pnas.1612208113
40. Brown NA, Bron AJ. An estimate of the human lens epithelial cell size in vivo. *Exp Eye Res*. 1987;44(6):899-906. doi:10.1016/S0014-4835(87)80052-0
41. Devalia J, Sapsford R, Wells C, Richman P, Davies R. Culture and comparison of human bronchial and nasal epithelial cells in vitro. *Respir Med*. 1990;84(4):303-312. doi:10.1016/S0954-6111(08)80058-3
42. Matsukawa Y, Lee VH, Crandall ED, Kim KJ. Size-dependent dextran transport across rat alveolar epithelial cell monolayers. *J Pharm Sci*. 1997;86(3):305-309. doi:10.1021/js960352x
43. Nicholson C, Syková E. Extracellular space structure revealed by diffusion analysis. *Trends Neurosci*. 1998;21(5):207-215. doi:10.1016/S0166-2236(98)01261-2
44. Syková E, Nicholson C. Diffusion in brain extracellular space. *Phys Rev*. 2008;88(4):1277-1340. doi:10.1152/physrev.00027.2007
45. McKee CT, Last JA, Russell P, Murphy CJ. Indentation versus tensile measurements of young's modulus for soft biological tissues. *Tissue Eng Pt B Rev*. 2011;17(3):155-164. doi:10.1089/ten.teb.2010.0520
46. Guimarães CF, Gasperini L, Marques AP, Reis RL. The stiffness of living tissues and its implications for tissue engineering. *Nature Rev Mater*. 2020;5(5):351-370. doi:10.1038/s41578-019-0169-1
47. Sahu P, Kang J, Erdemci-Tandogan G. Manning ML. Linear and nonlinear mechanical responses can be quite different in models for

biological tissues. *Soft Matter*. 2020;16(7):1850-1856. doi:10.1039/c9sm01068h

48. Parkins CC, McAbee JH, Ruff L, et al. Mechanically matching the rheological properties of brain tissue for drug-delivery in human glioblastoma models. *Biomaterials*. 2021;276:120919. doi:10.1016/j.biomaterials.2021.120919
49. Tuteja A, Mackay ME, Narayanan S, Asokan S, Wong MS. Breakdown of the continuum Stokes–Einstein relation for nanoparticle diffusion. *Nano Lett*. 2007;7(5):1276-1281. doi:10.1021/nl070192x
50. Cai LH, Panyukov S, Rubinstein M. Mobility of nonsticky nanoparticles in polymer liquids. *Macromolecules*. 2011;44(19):7853-7863. doi:10.1021/ma201583q
51. Griffiths AD, Tawfik DS. Miniaturising the laboratory in emulsion droplets. *Trends Biotechnol*. 2006;24(9):395-402. doi:10.1016/j.tibtech.2006.06.009
52. Helgeson ME. Colloidal behavior of nanoemulsions: interactions, structure, and rheology. *Curr Opin Colloid Interface Sci*. 2016;25:39-50. doi:10.1016/j.cocis.2016.06.006
53. Zetterlund PB, D'Hooge DR. The nanoreactor concept: kinetic features of compartmentalization in dispersed phase polymerization. *Macromolecules*. 2019;52(21):7963-7976. doi:10.1021/acs.macromol.9b01037
54. Moschakis T, Murray BS, Dickinson E. Particle tracking using confocal microscopy to probe the microrheology in a phase-separating emulsion containing nonadsorbing polysaccharide. *Langmuir*. 2006;22(10):4710-4719. doi:10.1021/la0533258
55. Guan J, Wang B, Granick S. Even hard-sphere colloidal suspensions display Fickian yet non-Gaussian diffusion. *ACS Nano*. 2014;8(4):3331-3336. doi:10.1021/nn405476t
56. Alam S, Mukhopadhyay A. Translational anisotropy and rotational diffusion of gold Nanorods in colloidal sphere solutions. *Langmuir*. 2015;31(32):8780-8785. doi:10.1021/acs.langmuir.5b01682
57. Sentjabrskaja T, Zaccarelli E, De Michele C, et al. Anomalous dynamics of intruders in a crowded environment of mobile obstacles. *Nat Commun*. 2016;7(1):11133. doi:10.1038/ncomms11133
58. Poling-Skutvik R, Roberts RC, Slim AH, et al. Structure dominates localization of tracers within aging nanoparticle glasses. *J Phys Chem Lett*. 2019;10(8):1784-1789. doi:10.1021/acs.jpclett.9b00309
59. Mei B, Schweizer KS. Activated penetrant dynamics in glass forming liquids: size effects, decoupling, slaving, collective elasticity and correlation with matrix compressibility. *Soft Matter*. 2021;17(9):2624-2639. doi:10.1039/d0sm02215b
60. Roberts RC, Poling-Skutvik R, Palmer JC, Conrad JC. Tracer transport probes relaxation and structure of attractive and repulsive glassy liquids. *J Phys Chem Lett*. 2018;9(11):3008-3013. doi:10.1021/acs.jpclett.8b01074
61. Skaug MJ, Wang L, Ding Y, Schwartz DK. Hindered nanoparticle diffusion and void accessibility in a three-dimensional porous medium. *ACS Nano*. 2015;9(2):2148-2156. doi:10.1021/acsnano.5b00019
62. He K, Babaye Khorasani F, Retterer ST, Thomas DK, Conrad JC, Krishnamoorti R. Diffusive dynamics of nanoparticles in arrays of nanoposts. *ACS Nano*. 2013;7(6):5122-5130. doi:10.1021/nn4007303
63. Raccis R, Nikoubashman A, Retsch M, et al. Confined diffusion in periodic porous nanostructures. *ACS Nano*. 2011;5(6):4607-4616. doi:10.1021/nn200767x
64. Rideau E, Dimova R, Schwille P, Wurm FR, Landfester K. Liposomes and polymersomes: a comparative review towards cell mimicking. *Chem Soc Rev*. 2018;47(23):8572-8610. doi:10.1039/c8cs00162f
65. Ivanov I, Castellanos SL, Balasbas S, et al. Bottom-up synthesis of artificial cells: recent highlights and future challenges. *Annu Rev Chem Biomol Eng*. 2021;12(1):287-308. doi:10.1146/annurev-chembioeng-092220-085918
66. Imai M, Sakuma Y, Kurisu M, Walde P. From vesicles toward protocells and minimal cells. *Soft Matter*. 2022;18(26):4823-4849. doi:10.1039/D1SM01695D
67. Utada AS, Lorenceau E, Link DR, Kaplan PD, Stone HA, Weitz DA. Monodisperse double emulsions generated from a microcapillary device. *Science*. 2005;308(5721):537-541. doi:10.1126/science.1109164
68. Chu LY, Utada AS, Shah RK, Kim JW, Weitz DA. Controllable monodisperse multiple emulsions. *Angew Chem*. 2007;119(47):9128-9132. doi:10.1002/ange.200701358
69. Zhang M, Corona PT, Ruocco N, et al. Controlling complex nanoemulsion morphology using asymmetric cosurfactants for the preparation of polymer nanocapsules. *Langmuir*. 2018;34(3):978-990. doi:10.1021/acs.langmuir.7b02843
70. Villar G, Graham AD, Bayley H. A tissue-like printed material. *Science*. 2013;340(6128):48-52. doi:10.1126/science.1229495
71. Baxani DK, Morgan AJL, Jamieson WD, Allender CJ, Barrow DA, Castell OK. Bilayer networks within a hydrogel shell: a robust chassis for artificial cells and a platform for membrane studies. *Angew Chem Int Ed*. 2016;55(46):14240-14245. doi:10.1002/anie.201607571
72. Booth MJ, Schild VR, Downs FG, Bayley H. Functional aqueous droplet networks. *Mol Biosyst*. 2017;13(9):1658-1691. doi:10.1039/C7MB00192D
73. Dupin A, Simmel FC. Signalling and differentiation in emulsion-based multi-compartmentalized in vitro gene circuits. *Nat Chem*. 2019;11(1):32-39. doi:10.1038/s41557-018-0174-9
74. Bayoumi M, Bayley H, Maglia G, Sapra KT. Multi-compartment encapsulation of communicating droplets and droplet networks in hydrogel as a model for artificial cells. *Sci Rep*. 2017;7(1):45167. doi:10.1038/srep45167
75. Kohli I, Mukhopadhyay A. Diffusion of nanoparticles in semidilute polymer solutions: effect of different length scales. *Macromolecules*. 2012;45(15):6143-6149. doi:10.1021/ma301237r
76. Kalwarczyk T, Sozanski K, Ochab-Marcinek A, et al. Motion of nanoprobes in complex liquids within the framework of the length-scale dependent viscosity model. *Adv Colloid Interface Sci*. 2015;223:55-63. doi:10.1016/j.cis.2015.06.007
77. Poling-Skutvik R, Krishnamoorti R, Conrad JC. Size-dependent dynamics of nanoparticles in Unentangled polyelectrolyte solutions. *ACS Macro Lett*. 2015;4(10):1169-1173. doi:10.1021/acsmacrolett.5b00616
78. Poling-Skutvik R, Mongcopa KIS, Faraone A, Narayanan S, Conrad JC, Krishnamoorti R. Structure and dynamics of interacting nanoparticles in semidilute polymer solutions. *Macromolecules*. 2016;49(17):6568-6577. doi:10.1021/acs.macromol.6b01277
79. Chen R, Poling-Skutvik R, Nikoubashman A, Howard MP, Conrad JC, Palmer JC. Coupling of nanoparticle dynamics to polymer center-of-mass motion in semidilute polymer solutions. *Macromolecules*. 2018;51(5):1865-1872. doi:10.1021/acs.macromol.7b02441
80. Schultz KM, Baldwin AD, Kiick KL, Furst EM. Gelation of covalently cross-linked PEG-heparin hydrogels. *Macromolecules*. 2009;42(14):5310-5315. doi:10.1021/ma900766u
81. Chen Y, Ma R, Qian X, et al. Nanoparticle mobility within permanently cross-linked polymer networks. *Macromolecules*. 2020;53(11):4172-4184. doi:10.1021/acs.macromol.0c00334
82. Parrish E, Caporizzo MA, Composto RJ. Network confinement and heterogeneity slows nanoparticle diffusion in polymer gels. *J Chem Phys*. 2017;146(20):203318. doi:10.1063/1.4978054
83. Cai LH, Panyukov S, Rubinstein M. Hopping diffusion of nanoparticles in polymer matrices. *Macromolecules*. 2015;48(3):847-862. doi:10.1021/ma501608x
84. Rose KA, Lee D, Composto RJ. pH-mediated nanoparticle dynamics in hydrogel nanocomposites. *Soft Matter*. 2021;17(10):2765-2774. doi:10.1039/d0sm02213f
85. Wehrman MD, Milstrey MJ, Lindberg S, Schultz KM. Using μ^2-rheology to quantify rheological properties during repeated reversible phase transitions of soft matter. *Lab Chip*. 2017;17:2085-2094. doi:10.1039/C7LC00222J

86. Guo H, Bourret G, Corbierre MK, et al. Nanoparticle motion within glassy polymer melts. *Phys Rev Lett*. 2009;102(7):075702. doi:10.1103/PhysRevLett.102.075702
87. Griffin PJ, Bocharova V, Middleton LR, et al. Influence of the bound polymer layer on nanoparticle diffusion in polymer melts. *ACS Macro Lett*. 2016;5(10):1141-1145. doi:10.1021/acsmacrolett.6b00649
88. Bailey EJ, Griffin PJ, Composto RJ, Winey KI. Multiscale dynamics of small, attractive nanoparticles and entangled polymers in polymer nanocomposites. *Macromolecules*. 2019;52(5):2181-2188. doi:10.1021/acs.macromol.8b02646
89. Keane DP, Mellor MD, Poling-Skutvik R. Responsive telechelic block copolymers for enhancing the elasticity of nanoemulsions. *ACS Appl Nano Mater*. 2022;5(5):5934-5943. doi:10.1021/acsanm.1c03666
90. Keane DP, Constantine CJ, Mellor MD, Poling-Skutvik R. Bridging heterogeneity dictates the microstructure and yielding response of polymer-linked emulsions. *Langmuir*. 2023;39(22):7852-7862. doi:10.1021/acs.langmuir.3c00707
91. Van Hove L. Correlations in space and time and born approximation scattering in systems of interacting particles. *Phys Rev*. 1954;95(1):249-262. doi:10.1103/PhysRev.95.249
92. Testard V, Julian-Oberdisse LC. Monte Carlo simulations of colloidal pair potential induced by telechelic polymers: statistics of loops and bridges. *Macromolecules*. 2008;41(19):7219-7226. doi:10.1021/ma8005813
93. Sprakel J, van der Gucht J, Cohen Stuart MA, Besseling NAM. Rouse dynamics of colloids bound to polymer networks. *Phys Rev Lett*. 2007;99(20):208301. doi:10.1103/PhysRevLett.99.208301
94. Rubinstein M, Colby RH. *Polymer Physics*. Oxford University Press; 2003.
95. Weeks ER, Crocker JC, Levitt AC, Schofield A, Weitz DA. Three-dimensional direct imaging of structural relaxation near the colloidal glass transition. *Science*. 2000;287(5453):627-631. doi:10.1126/science.287.5453.627
96. Weeks ER, Weitz DA. Properties of cage rearrangements observed near the colloidal glass transition. *Phys Rev Lett*. 2002;89(9):95704. doi:10.1103/PhysRevLett.89.095704
97. Jee AY, Curtis-Fisk JL, Granick S. Nanoparticle diffusion in methycellulose thermoreversible association polymer. *Macromolecules*. 2014;47(16):5793-5797. doi:10.1021/ma501331z
98. Lampo TJ, Stylianidou S, Backlund MP, Wiggins PA, Spakowitz AJ. Cytoplasmic RNA-protein particles exhibit non-Gaussian subdiffusive behavior. *Biophys J*. 2017;112(3):532-542. doi:10.1016/j.bpj.2016.11.3208
99. Slim AH, Poling-Skutvik R, Conrad JC. Local confinement controls diffusive nanoparticle dynamics in semidilute polyelectrolyte solutions. *Langmuir*. 2020;36(31):9153-9159. doi:10.1021/acs.langmuir.0c01402
100. Wang B, Anthony SM, Bae SC, Granick S. Anomalous yet Brownian. *Proc Natl Acad Sci U S A*. 2009;106(36):15160-15164. doi:10.1073/pnas.0903554106
101. Wang B, Kuo J, Bae SC, Granick S. When Brownian diffusion is not Gaussian. *Nat Mater*. 2012;11(6):481-485. doi:10.1038/nmat3308
102. Bajpai S, Tiwary SK, Sonker M, et al. Recent advances in nanoparticle-based cancer treatment: a review. *ACS App Nano Mater*. 2021;4(7):6441-6470. doi:10.1021/acsanm.1c00779
103. Ozdemir-Kaynak E, Qutub AA, Yesil-Celiktas O. Advances in glioblastoma multiforme treatment: new models for nanoparticle therapy. *Front Physiol*. 2018;9:170. doi:10.3389/fphys.2018.00170
104. Gravely M, Roxbury D. Multispectral fingerprinting resolves dynamics of nanomaterial trafficking in primary endothelial cells. *ACS Nano*. 2021;15(7):12388-12404. doi:10.1021/acsnano.1c04500
105. Joseph A, Nance E. Nanotherapeutics and the brain. *Annu Rev Chem Biomol Eng*. 2022;13(1):325-346. doi:10.1146/annurev-chembioeng-092220-030853

SUPPORTING INFORMATION

Additional supporting information can be found online in the Supporting Information section at the end of this article.

How to cite this article: Keane DP, Constantine CJ, Mellor MD, Poling-Skutvik R. Nanoparticle transport in biomimetic polymer-linked emulsions. *AIChE J*. 2023;e18307. doi:10.1002/aic.18307